RSC Advances

ROYAL SOCIETY OF CHEMISTRY

www.rsc.org/advances

Journal Name

RSCPublishing

ARTICLE

Graphene-based photocatalysts for oxygen evolution from water

Cite this: DOI: 10.1039/x0xx00000x

H. Pan[a], S. Zhu[a*], X. Lou[a], L. Mao[a], J. Lin[b], F. Tian[b], and D. Zhang[a]

Received 00th January 2014,
Accepted 00th January 2014

DOI: 10.1039/x0xx00000x

www.rsc.org/

Graphene (GR) has triggered new research field in material science, due to its unique monolayer structure, fascinating high conductivity, superior electron mobility, extremely high specific surface area and chemical stability. It is considered as an ideal matrix and electron mediator of semiconductor nanoparticles for environmental and energy application. Especially, GR-based nanocomposites have attracted significant attention when used as photocatalysts. This review will focus on oxygen evolution from water using GR-semiconductor photocatalytic system. Recent achievements of effective strategies in the fabrication of GR-based semiconductor photocatalysts for oxygen evolution from water are summarized. Furthermore, morphology control and composition design of the semiconductors on GR sheets are also reviewed in relation to the properties of photocatalytic oxygen generation. This review ends with a summary and some perspectives on major challenges and opportunities in the future research.

1. Introduction

Photocatalytic water splitting is of great importance, due to its efficient utilization of solar energy to chemical energy, which represents a promising technology to solve the global energy and environmental challenges[1-5]. Since the pioneered work reported by Honda[6], the concept of sunlight-induced H_2 or O_2 production has stimulated a large number of research efforts, leading to the development of numerous photocatalytic catalysts[7]. The semiconductor's band gap and electronic band edge positions with respect to water oxidation/reduction potential levels are very crucial in determining the feasibility of solar hydrogen/oxygen production. The ideal band gap of the semiconductors should be around 2.0 eV for the effective utilization of solar energy. Meanwhile, the bottom of the conduction band (CB) must be located at a more negative potential than the reduction potential (H^+/H_2), while the top of the valence band (VB) must be positioned more positively than the oxidation potential (H_2O/O_2)[8-10]. Unfortunately, rare semiconductor photocatalysts possess suitable redox potentials and band gaps for both simultaneous water reduction and oxidation. As a result, many researches have focused on half of the reaction by using sacrificial reagents as electron donors or acceptors, respectively[11]. Generally, hydrogen production from water reduction requires two electrons, while oxygen evolution from water oxidation is more challenging since it requires four holes to generate two oxygen-oxygen bonds for the production of per oxygen molecule[12-18]. That is the reason why the reported active photocatalysts for oxygen evolution from water are scarce, such as WO_3 and $BiVO_4$[19-21]. Recently, some new semiconductors, for instance, $BiCu_2VO_6$, $BiZn_2VO_6$, $TiN_xO_yF_z$, nitrogen-doped $CsCa_2Ta_3O_{10}$, layered double hydroxides (LDH) and Ag_3PO_4 crystals have also been investigated[22-27]. Obviously, oxygen evolution reaction is crucial for renewable energy technologies including water splitting and fuel cells[28]. Unfortunately, oxygen-evolving photocatalysts turn into the bottleneck for the development of energy-conversion schemes based on sunlight[29].

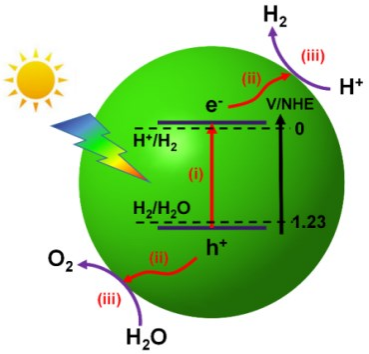

Figure 1. The principle and main process of photocatalytic oxygen generation from water.

The principle and main process of photocatalytic oxygen generation from water are schematically shown in Figure 1. Two key requirements should be considered for the fabrication of photocatalysts with efficient solar oxygen generation from water: one is excellent photo-adsorption ability within the solar spectrum, and the other is low recombination rate of photogenerated electron-hole pairs[1, 30-33]. In terms of the first issue, some semiconductors themselves possess efficient absorption in the visible-light solar spectrum, which occupies ~43% the solar radiation energy, such as Bi_2WO_6 and Bi_2MoO_6 with aurivillius structure, and $BiVO_4$ with a monoclinic scheelite structure[34-36]. However, most of these semiconductors are not ideal photocatalytic materials, because of their low quantum efficiency. A great deal of efforts have been made toward

improving the photocatalytic performance. Coupling with other substances to fabricate a semiconductor-based nanocomposite, such as the utilization of co-catalysts, Z-scheme photocatalysis, carbon quantum dots (CQD), and graphene (GR), is often taken as a feasible route for efficient photocatalysis[37-40]. Among them, semiconductor incorporated with GR has attracted considerable interest due to its unique properties[41]. With a flat monolayer of carbon atoms tightly packed into a two-dimensional honeycomb lattice, GR, possesses remarkable high conductivity, superior electron mobility and extremely high specific surface area (2630 m^2 g^{-1}), and can be produced on a large scale at low cost[42-44]. Given the excellent electronic conductivity endowed by its two-dimensional planar p-conjugation structure, GR in composites acts not only as a superior supporting matrix for bonding functional components but also as an excellent electron mediator to adjust electron transfer. Thus, it restrains the recombination of photoexcited charges and enhances the efficiency of electron-hole separation[45].

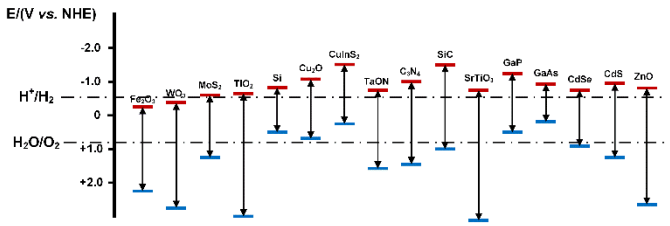

Figure 2. The conduction band and valence band positions of selected semiconductors (V *vs.* NHE, pH = 7). Reproduced from Ref. 8.

As is known, semiconductor possessing valence band position more positively than the oxidation potential (H_2O/O_2) is a potential photocatalyst for producing oxygen from water (Figure 2), such as WO_3, Fe_2O_3, TiO_2, ZnO, etc[46, 47]. When integrated with graphene, the unique characteristic of GR makes it more attractive in oxygen evolution. Photocatalytic systems, such as $BiWO_6$/GR, hematite/reduced graphene oxide (RGO), NiTi-LDH/RGO, WO_3/GR, $BiVO_4$/graphene oxide (GO) and Ag_3PO_4/Ag/AgBr/RGO, have been reported with greatly improved catalytic properties for oxygen evolution[48-53]. The combination of GR in photocatalyst has two obvious advantages: one is to widen light absorption range; the other one is to promote a stable catalytic system. For example, it is known that TiO_2 and ZnO can only be excited by ultraviolet (UV) or near UV radiation, owing to their wide band gaps. Inspiringly, the band gap energy values for these GR-based composites (GR nanosheets-TiO_2 and GR nanosheet-ZnO), are measured to be 1.39 and 1.26 eV, respectively. The narrowed band gap originated from GR makes this kind of composite a promising candidate for water splitting under sunlight[54]. Bai et al. found that the incorporation of GR could greatly enhance the stability of Ag_3PO_4, which is otherwise photocorrosive when used for photocatalytic O_2 production[55]. Additionally, the introduction of GR in WO_3 brings in an enhanced surface area and efficient separation of charges. It's worth mentioning that excess addition of GR would lead to a decrease in catalytic efficiency, because of the shielding effect of black GR on active sites.[56]

Thus, GR-based semiconductor photocatalysts have attracted extensive attention because of their usefulness in environmental and energy applications. This critical review summarizes the recent progress in the fabrication of GR-based semiconductor photocatalysts for oxygen evolution from water under visible-light irradiation. Morphology control and composition design of the semiconductors on GR sheets are reviewed in relation to the properties of photocatalytic oxygen generation. The importance of the interface between semiconductors and GR are highlighted. H_2 and O_2 evolution simultaneously from water by using GR-based materials is also discussed. This review ends with a summary and some perspectives on the challenges and new directions in this emerging area of research.

2. Synthesis of graphene-based photocatalysts

2.1. Solution mixing and *in situ* growth

Solution mixing is one of the most widely used methods to fabricate GR-based photocatalysts with easy operation and satisfiedresults obtained[41, 57]. To improve the photocatalytic properties, Ng *et al* fabricated WO_3/GR composite by mixing WO_3 powder with GR oxide (GO)[58]. WO_3 was added to the GO suspension and ultrasonicated for 30 min to produce a WO_3/GO dispersion. The dispersion was then exposed to either UV or visible light irradiation for 3 h to obtain WO_3/RGO composite. Although the morphological feature of WO_3/RGO composite was essentially identical, the WO_3 particle sizes were as large as 100 nm and tended to aggregate. Using the same strategy, WO_3/RGO composites were prepared by using polyvinylpyrrolidone (PVP) as an intermediate to combine tungsten with RGO. The mixture of GO and ammonium metatungstate hydrate was ultrasonicated and stirred to obtain WO_3/GO precursor solution. The resultant WO_3/RGO composite was obtained by calcining precursors at 450 °C for 5 h in air. As a result, WO_3 nanocrystallites ranged in 20-40 nm were uniformly distributed on the RGO[59].

In 2014, an *in situ* growth method was developed for the fabrication of visible-light-driven NiTi-LDH/RGO catalysts by anchoring NiTi-LDH nanosheets onto the surface of RGO, which displays excellent photocatalytic behaviour in water splitting into oxygen[50]. The monolayer RGO suspension was obtained by sonication in the deionized water. Titanium and nickel sources ($Ni(NO_3)_2{\cdot}6H_2O$, $TiCl_4$) and urea were dissolved in the RGO suspension. After stirring at 90 °C, the final precipitate was dried in an oven at 60 °C for 24 h. NiTi-LDH nanosheets on the surface of RGO are highly dispersed and have a plate-like morphology with a lateral diameter of 100-200 nm. The elemental mapping images display the uniform and homogeneous distribution of both Ni and Ti.

2.2. Hydrothermal and solvothermal approach

Apart from the approaches mentioned above, hydrothermal method is another efficient method for the synthesis of GR-based photocatalysts[60-62]. As compared with solution mixing method, hydrothermal and solvothermal approaches are more attractive, owing to their controllable morphology of semiconductor particles. More importantly, nanoparticles would be well bonded to GR even without any intermediate. Meng *et al* used hydrothermal process to prepare α-Fe_2O_3/RGO composite in which hematite nanoparticles are supported on the RGO nanosheets. A proper amount of $FeCl_3{\cdot}6H_2O$ was mixed with GO, and then the mixture was dissolved into deionized water and sonicated. Then, the prepared solution mixed with ethanol was placed in a boiling aqueous bath for thermal hydrolysis. The sample collected by centrifuging was heated in air at 350 °C for 2 h and then in pure nitrogen at 800 °C for 15 min. The crystalline size of monolithic α-Fe_2O_3 (63.8 nm) was larger than that of α-

Fe_2O_3 (41.4 nm) grown on the RGO sheets. The TEM image showed single-crystalline structure feature of α-Fe_2O_3 particle on the RGO sheet. The Fe_2O_3/RGO composite showed an enhanced photocatalytic activity toward water oxidation compared with the pristine α-Fe_2O_3 nanoparticles[49]. Similarly, Niu *et al* prepared RGO-cuprous oxide (Cu_2O/RGO) photocatalysts by using the same method. Well monodispersed cube-like Cu_2O particles (300-500 nm) were observed precipitation on the RGO layers[63]. Meanwhile, RGO/TiO_2 microspheres were produced by a non-hydrolytic sol-gel reaction of tetrabutyl orthotitanate (TBOT) and acetone followed by hydrothermal treatment[64]. The pretreated TiO_2 was prepared by adding TBOT in excess acetone. TiO_2/RGO microspheres were prepared by hydrothermal treatment in the temperature varied from 120 to 180 degrees. During the process, ammonia was used as a medium solution. It was found that the pre-treated TiO_2 was smooth and spherical in shape with particle diameter in the range between 1 and 2 μm. After treated at 120 °C, microspheres with aggregates of nanoflakes on the surface were produced. When the hydrothermal treatment temperature increased from 150 to 160 °C, rough microspheres with aggregates of nanorods were obtained. More recently, a solvothermal method was developed for the fabrication of Bi_2WO_6/RGO (BWO/RGO) composites. The mixture of GO, $Bi(NO_3)_3{\cdot}5H_2O$ and $Na_2WO_4{\cdot}2H_2O$ was sealed into a Teflon-lined autoclave and then maintained at 180 °C. Finally, Bi_2WO_6 nanoparticles deposited on the RGO sheets were produced, which showed some wrinkles. Obviously, solvothermal approach is widely used in fabrication of these GR-based photocatalysts. Unfortunately, most BWO particles were as large as a few hundreds of nanometers and their dispersion on GO sheets were not uniform, owing to the difficulty in controlling the composition and phase of the complex ternary compounds[65].

2.3. Sonochemical method

As mentioned above, the particle is more than several hundred nanometers in size on GR sheets by using the *in situ* growth method. Two key issues have to be considered for the design and fabrication of GR-based photocatalysts: (i) particle size control and (ii) interface between the catalysts and GR. How to control the particle size and improve the interaction between the semiconductor and GR is a challenge. In our previous work, the ultrasonic waves are proved to be effective to solve the problem[66-68]. Using ultrasonication we succeed in a controlled incorporation of TiO_2 nanoparticles onto GR layers homogeneously in a few hours. The average size of the nanoparticles is controlled at around 4-5 nm on the sheets without using any surfactant, which is attributed to the pyrolysis and condensation of the dissolved $TiCl_4$ into TiO_2 by ultrasonic waves. The uniform dispersion of TiO_2 nanoparticles on both the GR surface and the interlayers can be confirmed by SEM and TEM images. The results suggest ultrasound is very effective in dispersing TiO_2 nanoparticles on GR layers[68].

Inspired by the effective ultrasonic waves, we reported the synthesis of a composite (WO_3/GR) consisting of WO_3 nanoparticles and GR sheets using a sonochemical method. The average particle size of the WO_3 was controlled at around 12 nm on the GR sheets without using any surfactant. The composite consisted of nano-WO_3 particles and the two-dimensional GR sheets is a promising photocatalyst for oxygen production. When used as photocatalyst for water splitting, the amount of evolved O_2 from WO_3/GR with 40 wt% GR inside is much higher than that of pure WO_3 and mixed-WO_3/GR, 1.8 times and 2 times as much as that from mixed-WO_3/GR (*ca.* 214 mmol L^{-1}) and pure WO_3 (*ca.*186 mmol L^{-1}), respectively. The improved performance is due to the synergistic effects of chemically bondedWO_3 and GR. The sensitization of WO_3 by GR enhanced the visible light absorption property of WO_3/GR. Moreover, the chemical bonding between WO_3 and GR reduced the recombination of the photo-generated electron-hole pairs, leading to improved photoconversion efficiency. This simple strategy opens up a new way to design more optimized systems for photodissociating water under visible light. The same process has been extended to the fabrication of BWO on the surface of GR sheets. As is expected, the combination of functionality of BWO with the unique properties of GR results in an improved performance in O_2 production from water[51].

Additionally, some other approaches are developed to construct GR-based photocatalysts, such as layer-by-layer assembly, template-assisted approach, photoassisted method[69-73]. Usually, GR-based photocatalysts were prepared by the combination of above-mentioned methods, rather than individual of them.

3. Morphology control

As is well known, the morphology of semiconductors on GO plays a key point in photocatalytic performance. In our previous work, BWO nanoneedles was also fabricated on the surface of GR sheets by a facile sonochemical method followed with calcination[74]. The reduction of GR oxide plays an important role in fabricating nanoneedles (Fig. 3a, b) instead of nanoparticles on GR sheets. The oxygen-containing groups show strong influence on the morphology control of BWO on the surface of GR sheets. As compared with GO, RGO sheets have less quantity of oxygen-containing groups, providing less sites for both the physisorbtion of Bi ions and the deposition of BWO on the sheets, and this lead to the formation of BWO nanoneedles on the sheets after calcination (Fig. 3c). The nanoneedles have a cross-section area of ~450 nm at the bottom and a length of 2500 nm, and they form on the surface of GR sheets and disperse homogeneously. When used as photocatalyst for oxygen production, the oriented BWO grown on GR sheets produce oxygen of 188.9 μmol L^{-1}, higher than that of particulate BWO on GR (164.8 μmol/L). The high photocatalytic property is mainly attributed to the improved contact area of oriented BWO on GR sheets, resulting in increased active sites[75]. Similar results are obtained in photocatalytic systems of TiO_2 nanowire/GR and TiO_2 particle/GR.

It is widely recognized that a photocatalyst with high photocatalytic activity requires both high crystallinity and large surface area to reduce recombination of the photogenerated electron-hole and to increase the density of active surface sites, as well as to enhance the light harvesting. On the basis of the above consideration, exploring mesoporous materials as photocatalysts might be a significant subject since they not only possess the merits of both high crystallinity and large surface area, but also equip continuous pore channels to provide a short distance for photogenerated charge carrier transfer within the mesoporous frame work. In 2013, Huang *et al* reported a novel photocatalytic system by hybridizing GR with a mesoporous semiconductor for solar energy conversion[47]. The composite is composed of high-ordered mesoporous WO_3 (m-WO_3) and RGO. It is found that the obtained m-WO_3/RGO composite demonstrated a higher surface area and pore volume than that of m-WO_3. Furthermore, the specific surface area and pore volume increase with the increasing amount of RGO. Under visible light

irradiation, the amount of oxygen evolving from the optimized photocatalyst (*ca.* 6 wt% RGO) reaches 437.3 μmol g^{-1} in 5 h when KIO_3 was used as electron acceptor. In addition to the contribution of RGO, this superior photocatalytic activity could be ascribed to the mesoporous structure of m-WO_3, which provides large surface area and ordered meso-channels, thus more active sites could be achieved and charges could be efficiently transferred. Similar phenomenon is observed in C_3N_4/GR composite[76].

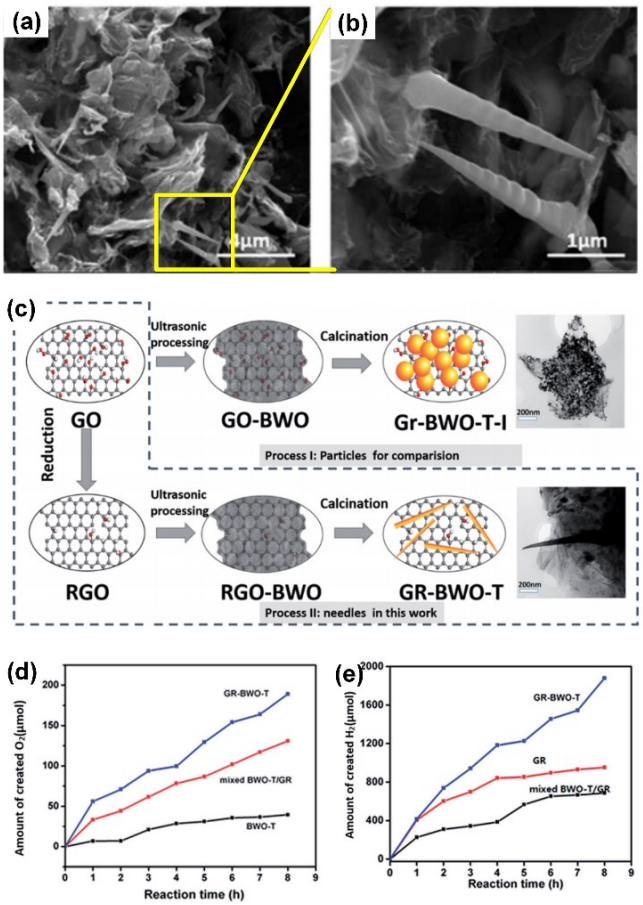

Figure 3. (a, b) The morphology of GO-BWO. (c) Proposed mechanism of the BWO-T nanoneedles' formation on GR sheets. (d, e) The photocatalytic O_2 (d) and H_2 (e) creation activities of Bi_2WO_6 powders (BWO-T), the physically mixed Bi_2WO_6 and the reduced GO (BWO-T/GR). Reproduced from Ref. 66.

4. Composition design

4.1. Nitrogen doping

GO is a p-doped material because oxygen atoms are more electronegative than carbon atoms[77]. However, GO itself shows a very small catalytic activity toward oxygen evolution from water. Doping with heteroatoms has been reported to alter the electrical properties, like nitrogen (N), which can induce a charge rearrangement on the GR sheets and enhance their catalytic activity[78]. Li *et al* reported the synthesis of N-doped GR (GN) by using nitrogen plasma treatment of GR and found that it exhibits high electrocatalytic activity for reduction of hydrogen peroxide and fast direct electron transfer kinetics for glucose oxidase[79].

More recently, Jing *et al* have prepared GR doped with different amounts of N through a one-pot ammonia-modified hydrothermal process and then successfully coupled them with nanocrystalline α-Fe_2O_3 by a common wet-chemical method[80].The increased amount of doped quaternary-type N would be quite favourable for photogenerated charge transfer and transportation. As a result, photogenerated charge separation of the resulting GN-Fe_2O_3nanocomposite is greatly promoted. This is responsible for the obviously improved visible activities of α-Fe_2O_3 for photoelectrochemical water oxidation to produce O_2. Interestingly, it is suggested for the first time that the increased amount of doped quaternary-type N would be very favourable for photogenerated charge transfer and transportation and for O_2 adsorption, further leading to the greatly increased charge separation in the resulting GN/Fe_2O_3nanocomposite. On the basis of the above results, it is reasonable to conclude that the photogenerated charge separation of α-Fe_2O_3 could be enhanced after coupling with a certain ratio of GR, especially with that doped with an appropriate amount of N species[81].

Similar result was found in the synthesis of GR modified with Fe and N (Fe-N-GR) by a rapid heat treatment possess[82]. N atoms are doped into the graphene planes and the reduction of GO is complete during the heat treatment. Fe atoms in the composite are supported by the doped N atoms *via* coordination bonds. The oxygen reduction reaction for the Fe-N-GR catalyst has an onset-potential of 850 mV *vs.* RHE (pH = 0.33).

4.2. Multicomponent synergism

As a new visible light photocatalyst for O_2 evolution from water, Ag_3PO_4, is unstable upon photo-illumination, which is easy to be corroded by the photogenerated electrons[26]. Compared with bare Ag_3PO_4, incorporating Ag_3PO_4 with GO not only improves photocatalytic activity, but also enhances the stability during photocatalytic process[83]. As is known, plasmon-mediated photocatalysis recently becomes a rising research star in the harvesting and conversion of solar energy, because photocatalysts containing semiconductors and plasmonic nanostructures of noble metals can enhance the photocatalytic activity primarily by extending the optical absorption region and enhancing the concentration of charge carriers through an excitation of surface plasmon resonance (SPR)[84]. In 2012, an Ag_3PO_4/Ag/AgBr/RGO hybrid composite with high visible light photocatalytic O_2-production activity was successfully prepared by a photoassisted deposition-precipitation strategy, followed by facile hydrothermal treatment[53]. Under irradiation with > 420 nm light, the effectiveness of these processes manifests itself in a 1.3 times higher O_2 evolution yield of Ag_3PO_4/Ag/AgBr/RGO as compared with that of Ag_3PO_4/Ag/AgBr and a 2 times higher yield compared with that of bare Ag_3PO_4 (Fig. 4a). The photocurrent traces show rapid response both at the start and at the end of illumination and an improved photocurrent density of the Ag_3PO_4/Ag/AgBr/RGO hybrid over all other composites (Fig. 4b). It is considered that the addition of Ag/AgBr caused conduction band depletion and valence band lowering of Ag_3PO_4; RGO supports this effect in a synergistic manner through delocalization of the transferred charge. Meanwhile, RGO provides significant parasitic absorption that partially counters the observed increase in efficiency. The mechanism is proposed as shown in Figure 4c. The as-synthesized N-doped Ag_3PO_4 nanoparticles are denuded of the majority of charge carriers by transfer to the Ag nanoparticles, eliminating the availability of extra conduction-band electrons for recombination with the photogenerated holes (resulting in increased hole availability for

water oxidation). This leads to the pinning of the Ag_3PO_4 conduction band at the silver Fermi level, shifting the Ag_3PO_4 valence band edge downward and rendering the photogenerated holes more active in water oxidation. Charge transferred to the silver creates a substantial negative charge on the very small metal nanoparticles, limiting their beneficial effect on the the photocatalyst. Charging of the nanoparticles can be reduced by distribution of the charge onto RGO sheets, further lowering the Ag_3PO_4 valence band position.

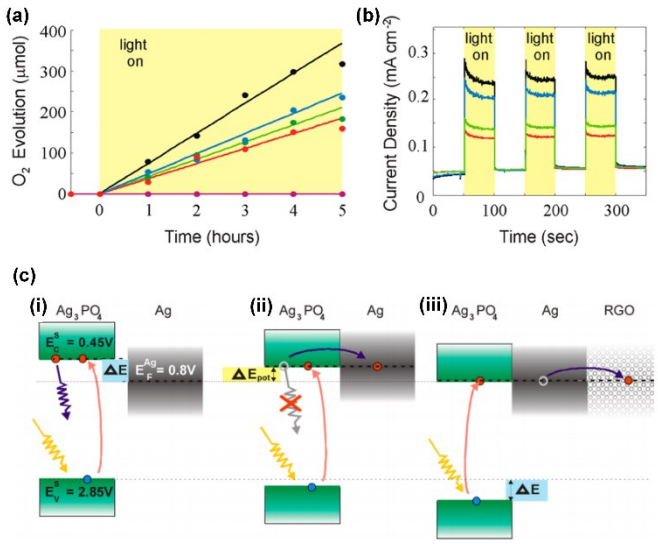

Figure 4. The photocatalytic performance of oxygen evolution and the photocatalytic mechanism model. (a) Photocatalytic O_2 production under visible light irradiation (λ > 420 nm) from a 0.05 M aqueous $AgNO_3$ solution over bare Ag/AgBr, Ag_3PO_4, Ag_3PO_4/RGO, Ag_3PO_4/Ag/AgBr, and Ag_3PO_4/Ag/AgBr/RGO (values 0, 38, 43, 48, 76 from bottom to top, unit μmol h^{-1}). (b) Transient photocurrent responses of electrodes functionalized with the Ag_3PO_4-based materials in the same order (bottom to top) as in panel (a). Measurements proceeded in a 0.01 M Na_2SO_4 aqueous solution under visible light irradiation (λ > 420 nm, I_0 = 64 mWcm^{-2}) at 0.5 V bias *vs* SCE. (c) Model of the synergistic increase of photocatalytic activity of Ag_3PO_4 upon functionalization with Ag/AgBr and RGO. Reprinted with permission from Ref. 77. Copyright 2012 American Chemical Society.

Further study was reported by Tian for the fabrication of CoPi nanoplates integrated with GO by photochemical deposition from an aqueous solution under visible-light illumination. Compared with GO, the CoPi/GO composites exhibit a 3.6-fold enhancement in the photocurrent. The photocurrent of the CoPi/GO-modified electrode after 2 h of illumination remained similar without any significant sign of catalyst dissolution or degradation. The GO not only serves as substrate for CoPi growth, but also increases charge transfer in the composites[73].

Additionally, some metal oxide has been employed as a co-catalyst to build novel semiconductor composites for photocatalysis, such as hausmannite (Mn_3O_4), a mixed valence manganese oxide. In 2014, Yin *et al* reported the fabrication of a nanocomposite consisting of α-Fe_2O_3, Mn_3O_4 and RGO for photocatalytic water oxidation to produce oxygen[85]. The a-Fe_2O_3/Mn_3O_4 hybrid prepared by modifying α-Fe_2O_3 with Mn_3O_4 nanoparticles was proved to anchor well on the two-dimensional RGO sheets of the nanocomposite, resulting in superior interfacial contacts between the hybrid and RGO. The typical p-type semiconductor Mn_3O_4 in the nanocomposite forms a heterojunction with α-Fe_2O_3 enhancing the charge transfer. In addition, Mn_3O_4 also acts as a noble-metal free co-catalyst reducing the oxygen evolution overpotential of hematite. RGO in the nanocomposite serves not only as a superior supporting matrix for anchoring the semiconductor nanoparticles but also as an excellent electron mediator to adjust electron transfer. As a result, the nanocomposite exhibited remarkably enhanced photocatalytic activity toward water oxidation compared with bare hematite or α-Fe_2O_3/Mn_3O_4 under UV-vis light irradiation. The quantum efficiency of the optimized photocatalystreached up to 4.35% at 365 nm.

4.3. Core/shell heterojunction structure

In addition to N-doping and multicomponent synergism system, core/shell geometry is another intriguing architecture which can improve the efficiency of energy conversion. With α-Fe_2O_3 nanorod cores, GR interlayer, and $BiV_{1-x}Mo_xO_4$ shells, a core/shell heterojunction array was fabricated by Hou *et al* for photoelectrochemical water splitting[86], shown in Figure 5a. The heterojunction yields a pronounced photocurrent density of ~1.97 mA cm^{-2} at 1.0 V *vs* Ag/AgCl and a high photoconversion efficiency of ~0.53% at -0.04 V *vs* Ag/AgCl under the irradiation of a Xe lamp (Fig. 5b). The unique core/shell architecture enhances the light absorption due to behaviour of the "window effect"[87] between the α-Fe_2O_3 cores and $BiV_{1-x}Mo_xO_4$ shells, and improves the separation of photogenerated carriers at α-Fe_2O_3/GR/$BiV_{1-x}Mo_xO_4$ interfaces.

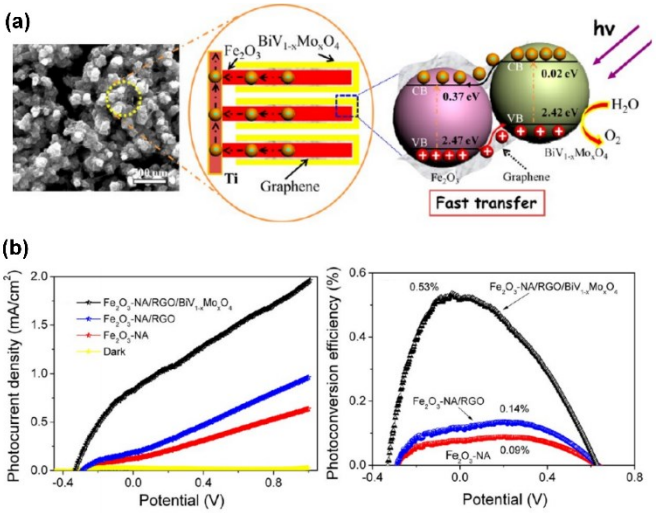

Figure 5. (a) Proposed mechanism of photoelectrochemical water splitting; (b) Variation of photocurrent density *vs* bias potential (left), and photoconversion efficiency as a function of applied potential (right).Reprinted with permission from Ref. 68. Copyright 2012 American Chemical Society.

5. Interface between semiconductors and graphene

It has been reported that the photoexcited electrons from TiO_2 transfer to nanocarbons, such as carbon nanotubes or GR, hinder the recombination process, thereby enhancing the oxidative reactivity[88, 89]. That is the reason why the GO-TiO_2 composites

exhibited excellent photochemical responses under visible light (>400 nm) irradiation. It was found that the unpaired p electrons on GO can bond with surface Ti atoms of TiO_2 to form Ti-O-C bonding and extend the light absorption range of TiO_2[90-92]. Further studies indicate that the interaction between GR and TiO_2 can significantly determine the interfacial electron transfer properties, which is a key issue for photocatalytic activity.

Similar phenomenon has been observed in Co_3O_4/N-doping RGO (Co_3O_4/N-RGO) composite with chemical bonding through a facile hydrothermal method[93]. X-ray absorption near edge structure (XANES) measurements were conducted to explore the interaction between GO and Co_3O_4. It was found that Co_3O_4/N-RGO hybrid exhibited an increase of carbon K-edge peak intensity at ~288 eV than pure N-RGO, corresponding to carbon atoms in GR attached to oxygen or other species. The result indicated the possible existence of Co-O-C or Co-N-C in the hybrid. Oxygen K-edge XANES and Co L-edge XANES measurements also suggest the same chemical bonding between two components. Liang's report demonstrated that the chemical bonding between GR and semiconductor could be achieved through a hydrothermal synthesis, which is relatively simple. The chemical bonding in GR-based photocatalysts could also be achieved through a simple sonochemical method, demonstrated by our previous fabrication of WO_3/GR used for photocatalytic oxygen evolution from water[51]. The bonding between WO_3 and GR minimizes the interface defects, reducing the recombination of photo-generated charges, responsible for the enhanced O_2 evolution.

Since the bridge facilitates charge transfer, and could be engineered through relatively simple method including hydrothermal or sonochemical synthesis. This kind of chemical bonding or other intimate interface are generally considered for GR-based photocatalysts architectures.

6. H_2 and O_2 evolution simultaneously from water by using graphene-based materials

As is known, semiconductor with large band gap or improper band location couldn't produce O_2 or H_2 effectively. In fact, rare semiconductor photocatalysts possess suitable redox potentials and band gaps for both simultaneous water reduction and oxidation. There are many reports about O_2 production from half reaction system containing sacrificial reagents, which is generally considered not accurately reflect their photocatalytic ability. In this part, GR-based photocatalytic systems which simultaneously produce O_2 and H_2 are introduced in detail.

6.1. Graphene oxide photocatalytic system

The electronic properties of GO are related to the composition of oxygen bonding on GR sheets[94]. The high electronegativity of oxygen atoms on carbon sheets causes the charge flow that exerts p-type semiconductivity to GO[95, 96]. As oxygen bonds on GR, the valence band changes from the π-orbital of GR to the O 2p orbital, leading to a larger band gap for a higher oxidation level of GO. Introducing more oxygen enlarges the band gap, and the valence band maximum (VBM) gradually changes from the p orbital of GR to the 2p orbital of oxygen; the p* orbital remains as the conduction band minimum (CBM). Yeh *et al* researched the electronic band energy levels of GO specimens with various oxidation levels using electrochemical methods[97]. The results reflect that with sufficient oxidation, the electronic structure of GO is proved suitable for both the reduction and oxidation of water under illumination, production of H_2 and O_2 gases in the presence of sacrificial reagents. They found the downward shift in the valence band edge was predominantly responsible for the enlargement of the band gap in the GO sheets. During photocatalytic reaction, the mutual reduction between GO sheets narrowed the band gap, leading to activity decay of GO in catalysing O_2 evolution from an $AgNO_3$ solution because of the upward shift of the valence band edge; whereas the activity for H_2 evolution from a methanol solution remained unchanged. A strong evolution of O_2 from a$NaIO_3$ solution under illumination was observed, probably due to more effective GO dispersion to suppress mutual reduction.

6.2. Z-Scheme system

Further study found that the combination of GO with Z-Scheme system makes it an effective mediator to produce H_2 and O_2 overall water splitting[52]. The GO was used as a solid-state redox mediator, and the $BiVO_4$ was used as an O_2-generating photocatalyst. The GO-$BiVO_4$ composite was mixed with a H_2-generating Ru-$SrTiO_3$:Rh photocatalyst in an aqueous solution with a pH value of 3.5 to enable inter-particulate contact. Under visible light irradiation, the photogenerated electrons transferred from the conduction band of $BiVO_4$ to GO for accumulation. When Ru-$SrTiO_3$:Rh contacted GO-$BiVO_4$, the accumulated electrons on GO transferred to Ru-$SrTiO_3$:Rh and combined with the photogenerated holes. The left electrons on Ru-$SrTiO_3$:Rh and the holes on $BiVO_4$ subsequently reacted with water, forming H_2 and O_2, respectively. The evolution of H_2 and O_2 in the stoichiometric ratio without decay indicated the occurrence of Z-scheme overall water splitting. The minimum turnover number (TON), which was calculated as the number of moles of reactive electrons per mole of GO, was 3.2 over 24h (Fig. 6a). The result suggested thephotoreduced GO (PRGO) is stable as a solid electron mediator and the Z-scheme system split water photocatalytically. The mechanism of water splitting in a Z-scheme photocatalysis system consisting of Ru/$SrTiO_3$:Rh and PRGO/$BiVO_4$ is shown in Figure 6b.

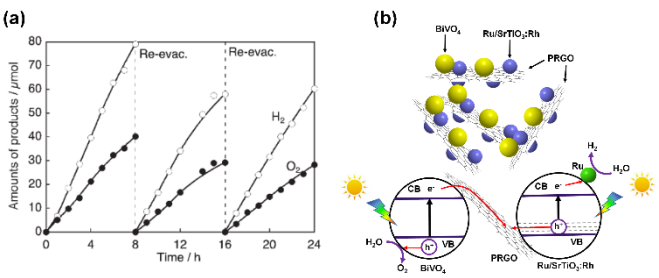

Figure 6. (a) Overall water splitting under visible-light irradiation by the (Ru/$SrTiO_3$:Rh)-(PRGO/$BiVO_4$) system. (b) Schematic image of a suspension of Ru/$SrTiO_3$ and PRGO/$BiVO_4$ in water (top); Mechanism of water splitting in a Z-scheme photocatalysis system consisting of Ru/$SrTiO_3$:Rh and PRGO/$BiVO_4$ under visible-light irradiation (down).Reprinted with permission from Ref. 89. Copyright 2011 American Chemical Society.

6.3. Graphene oxide quantum dots

Compared with 2D GR, graphene quantum dots (GQDs) as a kind of C-dots, exhibit new phenomena due to quantum confinement and edge effect[98]. GQDs have advantage that the

band gap of GQDs can be tuned from 0 eV to that of benzene by varying their sizes[99]. The incorporation of zero dimension GQDs could extend the photo-response of the photocatalyst to the visible-light range[100]. The combination of GQDs with photocatalyst, such as CdS-modified TiO_2 nanotube arrays (TNAs), ZnO nanowires and so on, were reported for photoelectrochemical water splitting[101, 102]. Very recently, Yeh *et al*. reported N-doped GO-quantum dots (NGO-QDs) as photocatalysts for overall water-splitting under visible light illumination[103]. The NGO-QDs exhibited both p- and n-type conductivities. Visible light (>420 nm) illumination on the NGO-QDs resulted in simultaneous H_2 and O_2 production from pure water at an H_2:O_2 molar ratio of 2:1 (Fig. 7a). Figure 7b shows time courses of H_2 production over the GO-QD photocatalysts, and no O_2 evolution was observed. Meanwhile, the evolution of O_2 over NH_3-NGO-QDs also cannot observe H_2 evolution (Fig. 7c). The results of Figure 7 (b and c) proved that the p- and n-domains were responsible for the evolution of H_2 and O_2, respectively. The authors suggested a p-n type photochemicaldiode configuration (Fig. 7d), which resulted in an energetic band bending existing at the interface between semiconductor and solution. The p-n type photochemicaldiode configuration provided a favourable situation to achieve vectorial charge displacement for overall water-splitting.

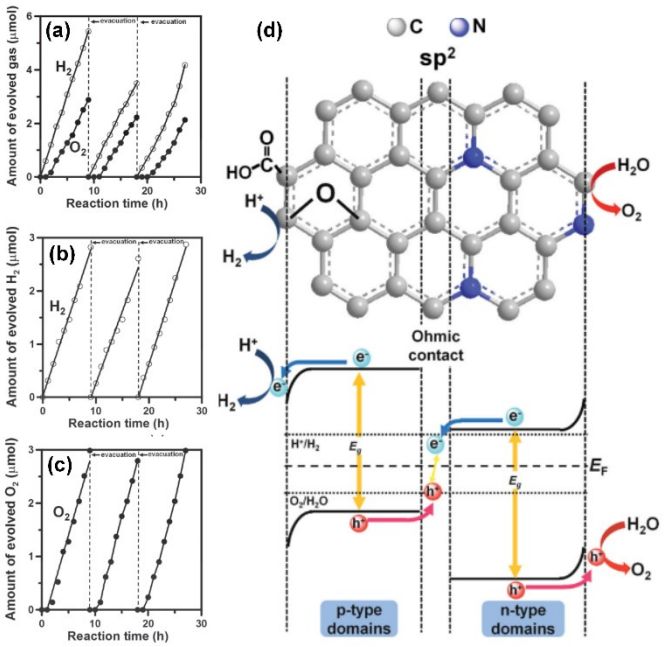

Figure 7. (a) Time courses of H_2 and O_2 evolution over 1.2 g NGO-QDs suspended in 200 mL of pure water under visible-light (420 nm < λ< 800 nm)irradiation. (b)Time courses of H_2 evolution over 1.2 g GO-QDs in the same condition of (a). (c) Time courses of O_2 evolution over 1.2 g NH_3-NGO-QDs in the same condition of (a). (d) The configuration and energy diagram for the NGO-QD photochemical diode. Reprinted with permission from Ref. 95. Copyright 2014 WILEY-VCH Verlag GmbH & Co. KGaA, Weinheim.

7. Summary and prospective

In summary, GR-based semiconductor photocatalysts for oxygen evolution from water attract much more attention as it is crucial for renewable energy technologies. Numbers approaches have been developed for the fabrication. The morphologies of semiconductors on GO influence the photocatalytic performance severely. Composition design is an effective method to enhance the photocatalytic properties, including nitrogen doping, multicomponent synergism system and core/shell heterojunction structure. With appropriate tuning of the CBM and VBM positions, the composites are suitable for H_2 and O_2 generation.

There are several challenges for researches on GO-based photocatalytic O_2 evolution from water. Firstly, theoretical electronic-structure calculations and experimental identification efforts are required. The dependence of photocatalytic properties on the particle size, layer number of GO should be explored, as they determine the charge transport mechanism in the GR-based composites.

Secondly, exploring and identify the interfacial contact and bonding between RGO and the semiconductors in the composites are needed[104]. The interaction of GR and semiconductor affects the morphology of the loaded particles which exert a strong influence on the photocatalytic performance of the resultant materials. On the other hand, the interface determines the efficiency of the electron-hole separation. To date, only a few techniques succeed in directly characterizing the interaction of GR and nanoparticles. Atomic resolution scanning transmission electron microscopy (STEM) and surface-enhanced Raman scattering (SERS) spectra may be the most potential techniques determining the interaction of GR-nanoparticles, although they only have been applied in metal-GR systems[105, 106].

Thirdly, studies on the preparation of a ternary hybrid as a photocatalyst for visible-light-driven water oxidation have been seldom reported[107, 108]. Especially, for the design of ternary hybrid with non-metal oxide, such as polymer. It has been reported that the preparation of PANI-GR-TiO_2 as a ternary hybrid, shows a remarkable photocatalytic activity and photostability for visible-light photoelectrocatalytic water oxidation[108]. Such a rationally designed ternary hybrid possesses unique advantages over traditional photocatalysts towards water oxidation.

The final challenge, is to design a structure for overall water splitting with simultaneous evolution of H_2 and O_2. Achieving this goal may require further exploiting GO, by chemically modifying it for example, to develop new nanostructured GO composites that efficiently transport charge inside the composites, and inject charges for reactions at the water-composite interface. All in all, a cheap, reliable and highly efficient photocatalyst for oxygen evolution is still needed to be exploited considering the critical role in the development of high performance energy conversion and storage devices.

8. Acknowledgements

The authors gratefully acknowledge the financial support of the National Science Foundation of China (NO. 51072117), Shanghai Science and Technology Committee (No. 13JC1403300). We also thank the Shanghai Jiao Tong University (SJTU) Instrument Analysis Center for the measurements.

Notes and references

[a]State Key Laboratory of Metal Matrix Composites, Shanghai Jiao Tong University, School of Materials Science and Engineering, Shanghai 200240, P R China.
[b]Shanghai Institute of Applied Physics Chines Academy of Sciences, Chinese Academy of Sciences, Shanghai 201204, P R China.
* Corresponding author, smzhu@sjtu.edu.cn

1. Z. G. Zou, J. H. Ye, K. Sayama and H. Arakawa, *Nature*, 2001, **414**, 625-627.
2. L. Z. Wu, B. Chen, Z. J. Li and C. H. Tung, *Accounts of Chemical Research*, 2014, **47**, 2177-2185.
3. F. Y. Song, Y. Ding and C. C. Zhao, *Acta Chimica Sinica*, 2014, **72**, 133-144.
4. P. Zhang, J. J. Zhang and J. L. Gong, *Chemical Society Reviews*, 2014, **43**, 4395-4422.
5. M. Matsuoka, M. Kitano, M. Takeuchi, K. Tsujimaru, M. Anpo and J. M. Thomas, *Catalysis Today*, 2007, **122**, 51-61.
6. K. H. A. Fujishima, *Nature*, 1972, **238**, 37-38.
7. A. Kudo and Y. Miseki, *Chemical Society Reviews*, 2009, **38**, 253-278.
8. J. Zhao, X. Wang, Z. C. Xu and J. S. C. Loo, *Journal of Materials Chemistry A*, 2014, **2**, 15228-15233.
9. X. Q. An and J. C. Yu, *Rsc Advances*, 2011, **1**, 1426-1434.
10. J. Yu, Y. Hai and B. Cheng, *The Journal of Physical Chemistry C*, 2011, **115**, 4953-4958.
11. Q. J. Xiang, J. G. Yu and M. Jaroniec, *Journal of the American Chemical Society*, 2012, **134**, 6575-6578.
12. K. Maeda, K. Teramura, D. L. Lu, T. Takata, N. Saito, Y. Inoue and K. Domen, *Nature*, 2006, **440**, 295-295.
13. K. Maeda, M. Higashi, B. Siritanaratkul, R. Abe and K. Domen, *Journal of the American Chemical Society*, 2011, **133**, 12334-12337.
14. K. Maeda, A. K. Xiong, T. Yoshinaga, T. Ikeda, N. Sakamoto, T. Hisatomi, M. Takashima, D. L. Lu, M. Kanehara, T. Setoyama, T. Teranishi and K. Domen, *Angewandte Chemie-International Edition*, 2010, **49**, 4096-4099.
15. X. B. Chen, S. H. Shen, L. J. Guo and S. S. Mao, *Chemical Reviews*, 2010, **110**, 6503-6570.
16. K. Maeda, M. Higashi, D. L. Lu, R. Abe and K. Domen, *Journal of the American Chemical Society*, 2010, **132**, 5858-5868.
17. M. W. Kanan and D. G. Nocera, *Science*, 2008, **321**, 1072-1075.
18. M. H. V. Huynh and T. J. Meyer, *Chemical Reviews*, 2007, **107**, 5004-5064.
19. J. X. Yang, D. G. Wang, X. Zhou and C. Li, *Chemistry-a European Journal*, 2013, **19**, 1320-1326.
20. J. A. Seabold and K. S. Choi, *Chemistry of Materials*, 2011, **23**, 1105-1112.
21. J. A. Seabold and K. S. Choi, *Journal of the American Chemical Society*, 2012, **134**, 2186-2192.
22. H. M. Liu, R. Nakamura and Y. Nakato, *Chemphyschem*, 2005, **6**, 2499-2502.
23. H. M. Liu, R. Nakamura and Y. Nakato, *Electrochemical and Solid State Letters*, 2006, **9**, G187-G190.
24. K. Maeda, B. J. Lee, D. L. Lu and K. Domen, *Chemistry of Materials*, 2009, **21**, 2286-2291.
25. X. Zong, C. H. Sun, Z. G. Chen, A. Mukherji, H. Wu, J. Zou, S. C. Smith, G. Q. Lu and L. Z. Wang, *Chemical Communications*, 2011, **47**, 6293-6295.
26. Z. G. Yi, J. H. Ye, N. Kikugawa, T. Kako, S. X. Ouyang, H. Stuart-Williams, H. Yang, J. Y. Cao, W. J. Luo, Z. S. Li, Y. Liu and R. L. Withers, *Nature Materials*, 2010, **9**, 559-564.
27. K. Maeda, Y. Shimodaira, B. Lee, K. Teramura, D. Lu, H. Kobayashi and K. Domen, *Journal of Physical Chemistry C*, 2007, **111**, 18264-18270.
28. A. A. Gewirth and M. S. Thorum, *Inorganic Chemistry*, 2010, **49**, 3557-3566.
29. J. L. Fillol, Z. Codola, I. Garcia-Bosch, L. Gomez, J. J. Pla and M. Costas, *Nature Chemistry*, 2011, **3**, 807-813.
30. K. Chang, Z. W. Mei, T. Wang, Q. Kang, S. X. Ouyang and J. H. Ye, *Acs Nano*, 2014, **8**, 7078-7087.
31. R. Marschall, *Advanced Functional Materials*, 2014, **24**, 2421-2440.
32. D. M. Schultz and T. P. Yoon, *Science*, 2014, **343**, 985-+.
33. R. Asahi, T. Morikawa, T. Ohwaki, K. Aoki and Y. Taga, *Science*, 2001, **293**, 269-271.
34. K. R. Lai, Y. T. Zhu, J. B. Lu, Y. Dai and B. B. Huang, *Computational Materials Science*, 2013, **67**, 88-92.
35. J. Q. Yu and A. Kudo, *Chemistry Letters*, 2005, **34**, 1528-1529.
36. H. M. Liu, R. Nakamura and Y. Nakato, *Journal of the Electrochemical Society*, 2005, **152**, G856-G861.
37. G. W. Busser, B. Mei, A. Pougin, J. Strunk, R. Gutkowski, W. Schuhmann, M. G. Willinger, R. Schlogl and M. Muhler, *Chemsuschem*, 2014, **7**, 1030-1034.
38. Y. X. Yang, W. Guo, Y. N. Guo, Y. H. Zhao, X. Yuan and Y. H. Guo, *Journal of Hazardous Materials*, 2014, **271**, 150-159.
39. M. Miyauchi, Y. Nukui, D. Atarashi and E. Sakai, *Acs Applied Materials & Interfaces*, 2013, **5**, 9770-9776.
40. H. J. Yu, Y. F. Zhao, C. Zhou, L. Shang, Y. Peng, Y. H. Cao, L. Z. Wu, C. H. Tung and T. R. Zhang, *Journal of Materials Chemistry A*, 2014, **2**, 3344-3351.
41. Q. J. Xiang, J. G. Yu and M. Jaroniec, *Chemical Society Reviews*, 2012, **41**, 782-796.
42. C. Lee, X. D. Wei, J. W. Kysar and J. Hone, *Science*, 2008, **321**, 385-388.
43. A. A. Balandin, S. Ghosh, W. Z. Bao, I. Calizo, D. Teweldebrhan, F. Miao and C. N. Lau, *Nano Letters*, 2008, **8**, 902-907.
44. Y. W. Zhu, S. Murali, W. W. Cai, X. S. Li, J. W. Suk, J. R. Potts and R. S. Ruoff, *Advanced Materials*, 2010, **22**, 3906-3924.
45. L. Mao, S. M. Zhu, J. Ma, D. A. Shi, Y. X. Chen, Z. X. Chen, C. Yin, Y. Li and D. Zhang, *Nanotechnology*, 2014, **25**.
46. M. J. Zhou, N. Zhang and Z. H. Hou, *International Journal of Photoenergy*, 2014.
47. H. Huang, Z. K. Yue, G. Li, X. M. Wang, J. Huang, Y. K. Du and P. Yang, *Journal of Materials Chemistry A*, 2013, **1**, 15110-15116.
48. Z. H. Sun, J. J. Guo, S. M. Zhu, L. Mao, J. Ma and D. Zhang, *Nanoscale*, 2014, **6**, 2186-2193.
49. F. K. Meng, J. T. Li, S. K. Cushing, J. Bright, M. J. Zhi, J. D. Rowley, Z. L. Hong, A. Manivannan, A. D. Bristow and N. Q. Wu, *Acs Catalysis*, 2013, **3**, 746-751.
50. B. Li, Y. F. Zhao, S. T. Zhang, W. Gao and M. Wei, *Acs Applied Materials & Interfaces*, 2013, **5**, 10233-10239.
51. J. J. Guo, Y. Li, S. M. Zhu, Z. X. Chen, Q. L. Liu, D. Zhang, W. J. Moon and D. M. Song, *Rsc Advances*, 2012, **2**, 1356-1363.
52. A. Iwase, Y. H. Ng, Y. Ishiguro, A. Kudo and R. Amal, *Journal of the American Chemical Society*, 2011, **133**, 11054-11057.
53. Y. Hou, F. Zuo, Q. Ma, C. Wang, L. Bartels and P. Y. Feng, *Journal of Physical Chemistry C*, 2012, **116**, 20132-20139.
54. R. A. Rakkesh, D. Durgalakshmi and S. Balakumar, *Journal of Materials Chemistry C*, 2014, **2**, 6827-6834.
55. S. Bai, X. P. Shen, H. W. Lv, G. X. Zhu, C. L. L. Bao and Y. X. Shan, *Journal of Colloid and Interface Science*, 2013, **405**, 1-9.
56. Q. Li, B. D. Guo, J. G. Yu, J. R. Ran, B. H. Zhang, H. J. Yan and J. R. Gong, *Journal of the American Chemical Society*, 2011, **133**, 10878-10884.
57. J. F. Dai, T. Xian, L. J. Di and H. Yang, *Journal of Nanomaterials*, 2013.
58. Y. H. Ng, A. Iwase, N. J. Bell, A. Kudo and R. Amal, *Catalysis Today*, 2011, **164**, 353-357.
59. J. D. Lin, P. Hu, Y. Zhang, M. T. Fan, Z. M. He, C. K. Ngaw, J. S. C. Loo, D. W. Liao and T. T. Y. Tan, *Rsc Advances*, 2013, **3**, 9330-9336.
60. X. F. Yang, H. Y. Cui, Y. Li, J. L. Qin, R. X. Zhang and H. Tang, *Acs Catalysis*, 2013, **3**, 363-369.
61. S. Y. Dong, Y. R. Cui, Y. F. Wang, Y. K. Li, L. M. Hu, J. Y. Sun and J. H. Sun, *Chemical Engineering Journal*, 2014, **249**, 102-110.
62. Y. Hou, X. Y. Li, Q. D. Zhao and G. H. Chen, *Applied Catalysis B-Environmental*, 2013, **142**, 80-88.
63. Z. G. Niu, *Materials Science in Semiconductor Processing*, 2014, **23**, 78-84.
64. P. T. N. Nguyen, C. Salim, W. Kurniawan and H. Hinode, *Catalysis Today*, 2014, **230**, 166-173.
65. J. J. Xu, Y. H. Ao and M. D. Chen, *Materials Letters*, 2013, **92**, 126-128.
66. S. M. Zhu, J. J. Guo, J. P. Dong, Z. W. Cui, T. Lu, C. L. Zhu, D. Zhang and J. Ma, *Ultrasonics Sonochemistry*, 2013, **20**, 872-880.
67. S. M. Zhu, C. L. Zhu, J. Ma, Q. Meng, Z. P. Guo, Z. Y. Yu, T. Lu, Y. Li, D. Zhang and W. M. Lau, *Rsc Advances*, 2013, **3**, 6141-6146.
68. J. J. Guo, S. M. Zhu, Z. X. Chen, Y. Li, Z. Y. Yu, Q. L. Liu, J. B. Li, C. L. Feng and D. Zhang, *Ultrasonics Sonochemistry*, 2011, **18**, 1082-1090.

69. B. H. R. Suryanto, X. Y. Lu and C. Zhao, *Journal of Materials Chemistry A*, 2013, **1**, 12726-12731.
70. S. Y. Dong, Y. K. Li, J. Y. Sun, C. F. Yu, Y. H. Li and J. H. Sun, *Materials Chemistry and Physics*, 2014, **145**, 357-365.
71. C. Lavorato, A. Primo, R. Molinari and H. Garcia, *Acs Catalysis*, 2014, **4**, 497-504.
72. W. Yan, F. He, S. L. Gai, P. Gao, Y. J. Chen and P. P. Yang, *Journal of Materials Chemistry A*, 2014, **2**, 3605-3612.
73. J. Q. Tian, H. Y. Li, A. M. Asiri, A. O. Al-Youbi and X. P. Sun, *Small*, 2013, **9**, 2709-2714.
74. Z. H. Sun, J. J. Guo, S. M. Zhu, J. Ma, Y. L. Liao and D. Zhang, *Rsc Advances*, 2014, **4**, 27963-27970.
75. X. Pan, Y. Zhao, S. Liu, C. L. Korzeniewski, S. Wang and Z. Y. Fan, *Acs Applied Materials & Interfaces*, 2012, **4**, 3944-3950.
76. Q. J. Xiang, J. G. Yu and M. Jaroniec, *Journal of Physical Chemistry C*, 2011, **115**, 7355-7363.
77. X. R. Wang, X. L. Li, L. Zhang, Y. Yoon, P. K. Weber, H. L. Wang, J. Guo and H. J. Dai, *Science*, 2009, **324**, 768-771.
78. L. Ci, L. Song, C. H. Jin, D. Jariwala, D. X. Wu, Y. J. Li, A. Srivastava, Z. F. Wang, K. Storr, L. Balicas, F. Liu and P. M. Ajayan, *Nature Materials*, 2010, **9**, 430-435.
79. Y. Wang, Y. Y. Shao, D. W. Matson, J. H. Li and Y. H. Lin, *Acs Nano*, 2010, **4**, 1790-1798.
80. L. M. He, L. Q. Jing, Y. B. Luan, L. Wang and H. G. Fu, *Acs Catalysis*, 2014, **4**, 990-998.
81. Y. J. Wang, R. Shi, J. Lin and Y. F. Zhu, *Applied Catalysis B-Environmental*, 2010, **100**, 179-183.
82. K. Kamiya, K. Hashimoto and S. Nakanishi, *Chemical Communications*, 2012, **48**, 10213-10215.
83. L. Liu, J. C. Liu and D. D. Sun, *Catalysis Science & Technology*, 2012, **2**, 2525-2532.
84. S. Linic, P. Christopher and D. B. Ingram, *Nature Materials*, 2011, **10**, 911-921.
85. S. L. Yin, X. M. Wang, Z. G. Mou, Y. J. Wu, H. Huang, M. S. Zhu, Y. K. Du and P. Yang, *Physical Chemistry Chemical Physics*, 2014, **16**, 11289-11296.
86. Y. Hou, F. Zuo, A. Dagg and P. Y. Feng, *Nano Letters*, 2012, **12**, 6464-6473.
87. H. T. Yu, S. Chen, X. Quan, H. M. Zhao and Y. B. Zhang, *Applied Catalysis B-Environmental*, 2009, **90**, 242-248.
88. G. X. Wang, B. Wang, J. Park, J. Yang, X. P. Shen and J. Yao, *Carbon*, 2009, **47**, 68-72.
89. G. Williams, B. Seger and P. V. Kamat, *Acs Nano*, 2008, **2**, 1487-1491.
90. H. Zhang, X. J. Lv, Y. M. Li, Y. Wang and J. H. Li, *Acs Nano*, 2010, **4**, 380-386.
91. I. Y. Kim, J. M. Lee, T. W. Kim, H. N. Kim, H. I. Kim, W. Choi and S. J. Hwang, *Small*, 2012, **8**, 1038-1048.
92. J. S. Lee, K. H. You and C. B. Park, *Advanced Materials*, 2012, **24**, 1084-1088.
93. Y. Y. Liang, Y. G. Li, H. L. Wang, J. G. Zhou, J. Wang, T. Regier and H. J. Dai, *Nature Materials*, 2011, **10**, 780-786.
94. R. J. W. E. Lahaye, H. K. Jeong, C. Y. Park and Y. H. Lee, *Physical Review B*, 2009, **79**.
95. J. Ito, J. Nakamura and A. Natori, *Journal of Applied Physics*, 2008, **103**.
96. G. H. Lu, L. E. Ocola and J. H. Chen, *Nanotechnology*, 2009, **20**.
97. T. F. Yeh, F. F. Chan, C. T. Hsieh and H. S. Teng, *Journal of Physical Chemistry C*, 2011, **115**, 22587-22597.
98. J. H. Shen, Y. H. Zhu, X. L. Yang and C. Z. Li, *Chemical Communications*, 2012, **48**, 3686-3699.
99. Y. W. Son, M. L. Cohen and S. G. Louie, *Physical Review Letters*, 2006, **97**.
100. D. K. L. Chan, P. L. Cheung and J. C. Yu, *Beilstein Journal of Nanotechnology*, 2014, **5**, 689-695.
101. Y. F. Yu, J. L. Ren and M. Meng, *International Journal of Hydrogen Energy*, 2013, **38**, 12266-12272.
102. C. X. Guo, Y. Q. Dong, H. B. Yang and C. M. Li, *Advanced Energy Materials*, 2013, **3**, 997-1003.
103. T. F. Yeh, C. Y. Teng, S. J. Chen and H. S. Teng, *Advanced Materials*, 2014, **26**, 3297-+.
104. E. Gracia-Espino, G. Z. Hu, A. Shchukarev and T. Wagberg, *Journal of the American Chemical Society*, 2014, **136**, 6626-6633.
105. J. Lee, K. S. Novoselov and H. S. Shin, *Acs Nano*, 2011, **5**, 608-612.
106. R. Zan, U. Bangert, Q. Ramasse and K. S. Novoselov, *Nano Letters*, 2011, **11**, 1087-1092.
107. W. J. Han, L. Ren, X. Qi, Y. D. Liu, X. L. Wei, Z. Y. Huang and J. X. Zhong, *Applied Surface Science*, 2014, **299**, 12-18.
108. L. Jing, Z. Y. Yang, Y. F. Zhao, Y. X. Zhang, X. Guo, Y. M. Yan and K. N. Sun, *Journal of Materials Chemistry A*, 2014, **2**, 1068-1075.

TOC:

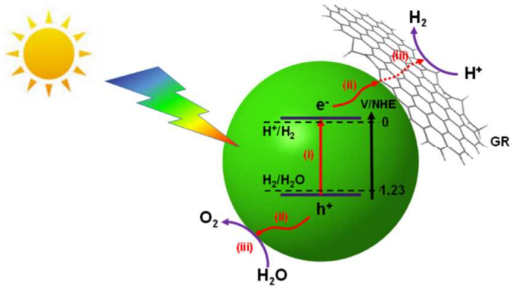

Recent achievements of GR-based photocatalysts for oxygen evolution from water are summarized, with perspectives on major challenges and opportunities.

S. Zhu received her PhD degree in Shanghai Jiaotong University in 2001. She presently is a professor in School of Materials Science and Engineering, State Key Lab of Metal Matrix Composites, Shanghai Jiao Tong University. Her current field of interest is graphene-based functional materials, porous carbon, and biomimetic materials based on biological templates.

H. Pan received his master degree from Donghua University at State Key Laboratory for Modification of Chemical Fibers and Polymer Materials, College of Materials Science and Engineering in 2014. Presently he is a PhD student under the supervision of Professor S. Zhu. His current work focuses on graphene-based functional materials.